Int J Adv Manuf Technol (2013) 66:537–545
DOI 10.1007/s00170-012-4347-1

ORIGINAL ARTICLE

Parallel grinding error for a noncoaxial nonaxisymmetric aspheric lens using a fixture with adjustable gradient

Chen Jiang · Yinbiao Guo · Haolin Li

Received: 12 January 2012 / Accepted: 22 June 2012 / Published online: 10 July 2012

Abstract To machine a noncoaxial nonaxisymmetric aspheric lens, a new parallel grinding method that employs a fixture with an adjustable gradient (AGF) is proposed. The AGF is developed for a three-axis computer numerically controlled grinding machine. The grinding method is presented according to the proposed grinding system. To ensure the machining accuracy, the main machining errors and the compensation algorithm are discussed for the grinding method using the AGF. Simulation results show that the AGF rotation errors are crucial factors affecting the profile error of the machined workpiece. Experimental results show that employing the compensation algorithm increases machining accuracy.

Keywords Noncoaxial nonaxisymmetric aspheric · Parallel grinding · Fixture · Error compensation

1 Introduction

With the development of optic and photonic industries, the high-quality optical aspheric lens is playing increasingly important functional roles in many key instruments, such as satellites, telescopes, and cameras [1–5]. The noncoaxial nonaxisymmetric aspheric lens (NNAL), which is a combination of a nonaxisymmetric aspheric lens and a prism, is widely used in high-performance optical systems because it simplifies the optical system and decreases the number of system components.

Recently, ultraprecision grinding technology of aspheric parts has developed rapidly. Some researchers have developed many new tools and methods to ensure the machining accuracy and efficiency. Chen et al. [6] have developed an ultraprecision aspheric grinding system to machining the large depth-to-diameter ratio aspheric parts. Cheng et al. [7] have designed a six-axis machining system, which has the features of conventional loose abrasive machining with the characteristics of a tool having multiple degrees of freedom moving in planar model. Lee et al. [8] have developed an ultraprecision grinding system for manufacturing the aspheric surface microlens by considering the factors affecting the grinding surface roughness and profile accuracy. Xie et al. [9] have proposed an applicable algorithm of 3D tool paths for computer numerically controlled (CNC) envelope grinding of an arbitrary free-form surface. And further, to verify 3D distribution of envelop traces and form errors on ground curve surface, they [10] proposed a new simulation method for envelope grinding of nonaxisymmetric aspheric surface by using 3D virtual curve grinding. Lee et al. [11] have proposed a precise-arc interpolation method, which can meet the given tolerance precisely, to minimize the error induced by the cutting tool path and to shorten the calculation time of interpolation. Chen et al. [12] have proposed a compensation approach based on the on-machine measurement for the grinding of aspheric parts. The profile error after grinding was obtained by subtracting the target profile from the actual ground profile along normal direction and was then used to generate a new tool path for compensation grinding.

C. Jiang (✉) · H. Li
College of Mechanical Engineering, University of Shanghai for Science and Technology,
Shanghai 200093, China
e-mail: jc_bati@yahoo.com.cn

H. Li
e-mail: haolin61@163.com

Y. Guo
Department of Mechanical and Electrical Engineering,
Xiamen University,
Xiamen 361005, China
e-mail: guoyb@xmu.edu.cn

Although the precision grinding methods for manufacturing of aspheric surface are developed, it has not yet been reported about an applicable method of grinding for the NNAL. In the conventional machining method, the incline of the aspheric surface of the NNAL affects the uniform distribution of machining errors across the aspheric surface of workpiece. To ensure a uniform distribution of machining errors and to improve machining efficiency, a fixture with an adjustable gradient (AGF) is designed to cooperate with a three-axis CNC grinding machine in machining the NNAL. The parallel grinding method [13, 14] is adopted to simplify the machining processing and to minimize the profile error caused by wheel wear in the grinding process. In this work, the error analysis of an AGF in the parallel grinding method is discussed and a compensation algorithm is presented.

2 Grinding system and method

A typical structure of an NNAL is shown in Fig. 1. The NNAL comprises a nonaxisymmetric aspheric lens and a prism according to the required characteristics of the optical system. The formula for the nonaxisymmetric aspheric surface of the NNAL is:

$$y(x,z) = -R_x + \sqrt{R_x^2 - x^2} + \frac{C_s z^2}{1 + \sqrt{1 - (1+k)C_s^2 z^2}}, \quad (1)$$

$$C_s = 1/R_s, \quad (2)$$

$$R_s = -R_z + Ax^2 + Bx^4 + Cx^6 + Dx^8 + Ex^{10} + Fx^{12}, \quad (3)$$

where R_s is the radius of the aspheric secondary axis; R_x is the basic radius of the aspheric main axis; R_z is the basic radius of the aspheric secondary axis; k is the aspheric coefficient; and A, B, C, D, E, and F are aspheric secondary axis coefficients. Another important parameter of the NNAL is the wedge angle θ as shown in Fig. 1.

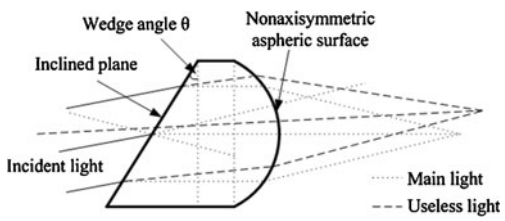

Fig. 1 Structure of the NNAL

2.1 Grinding system and the AGF

Figure 2a is a structural diagram of the three-axis CNC grinding machine, which is applied to machine the NNAL. Figure 2b is a schematic diagram of the AGF, and Fig. 2c is a photograph of the AGF. The platform of the AGF, which is used to fix the workpiece, can rotate around the A, B, and C axes to satisfy the machining requirement of the NNAL. The rotation of the AGF platform is driven by a built-in three-axis servo system. Rotation about the A, B, and C axes is limited to ±4°, ±8°, and ±16°, respectively. The resolution of rotation is 0.01° and relates to the servomotor and reducer.

2.2 Parallel grinding method using the AGF

Compared with the grinding process for a conventional nonaxisymmetric aspheric lens, the grinding process for the NNAL is more complex owing to the inclined plane of the lens. However, the AGF can simplify the machining process and improve the machining efficiency. The AGF platform can rotate about the A, B, and C axes according to the machining requirement. When the workpiece is fixed on the AGF platform, the workpiece can be tilted from the horizontal according to the wedge angle of the workpiece as shown in Fig. 3a. Therefore, the nonaxisymmetric aspheric surface of the NNAL can be ground as for the general nonaxisymmetric aspheric lens without an inclined plane. Moreover, the rough grinding of the inclined plane is bypassed. A uniform distribution of machining errors for the surface of the workpiece is thus effectively ensured.

In conventional grinding of a nonaxisymmetric aspheric workpiece, the tool path is a plane curve parallel to the XOY plane in the locus plan of linear interpolation. Only one part of the wheel is used in this grinding process. Therefore, wheel wear is localized at this point. Moreover, it is impossible to grind a large workpiece because of the collision between the wheel head and workpiece. To solve this problem, the parallel grinding method is applied by means of an arc wheel. In parallel grinding, the arc profile of the wheel is dressed to the shape of circular arc. Figure 3b shows that the arc wheel has two main geometry parameters including the arc radius r and the basic radius R. r is the radius of wheel arc profile, and R is the radius of basic round of the arc wheel. Figure 3a shows that the basic round of the arc wheel is the locus of center of the wheel arc profile. As shown in Fig. 3b, the normal direction of contacted position on the wheel surface is always opposite to the normal direction of contacted position on the workpiece surface for each interpolation point. Therefore, the grinding point changes along the wheel arc profile with each grinding pass. Furthermore, the parallel grinding method has the advantage that surface roughness improves because there are more active cutting edges than in the conventional method.

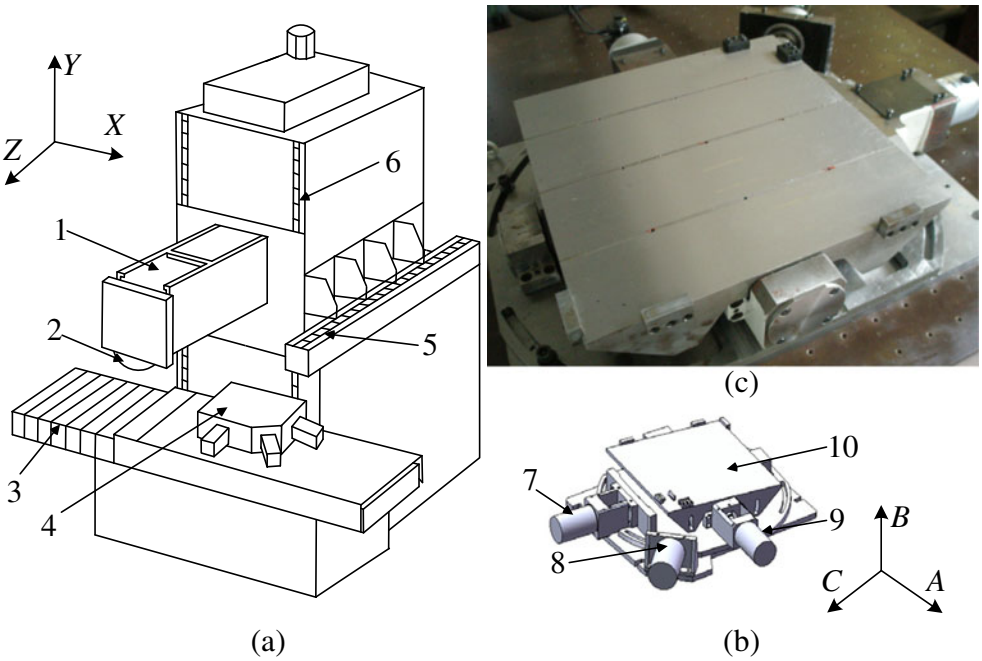

Fig. 2 **a**–**c** Three-axis CNC machining machine and the AGF. *1*, main spindle; *2*, arc wheel; *3*, *X* axis guideways; *4*, AGF; *5*, *Z* axis guideways; *6*, *Y* axis guideways; *7*, *C* axis motor; *8*, *B* axis motor; *9*, *A* axis motor; *10*, platform of the AGF

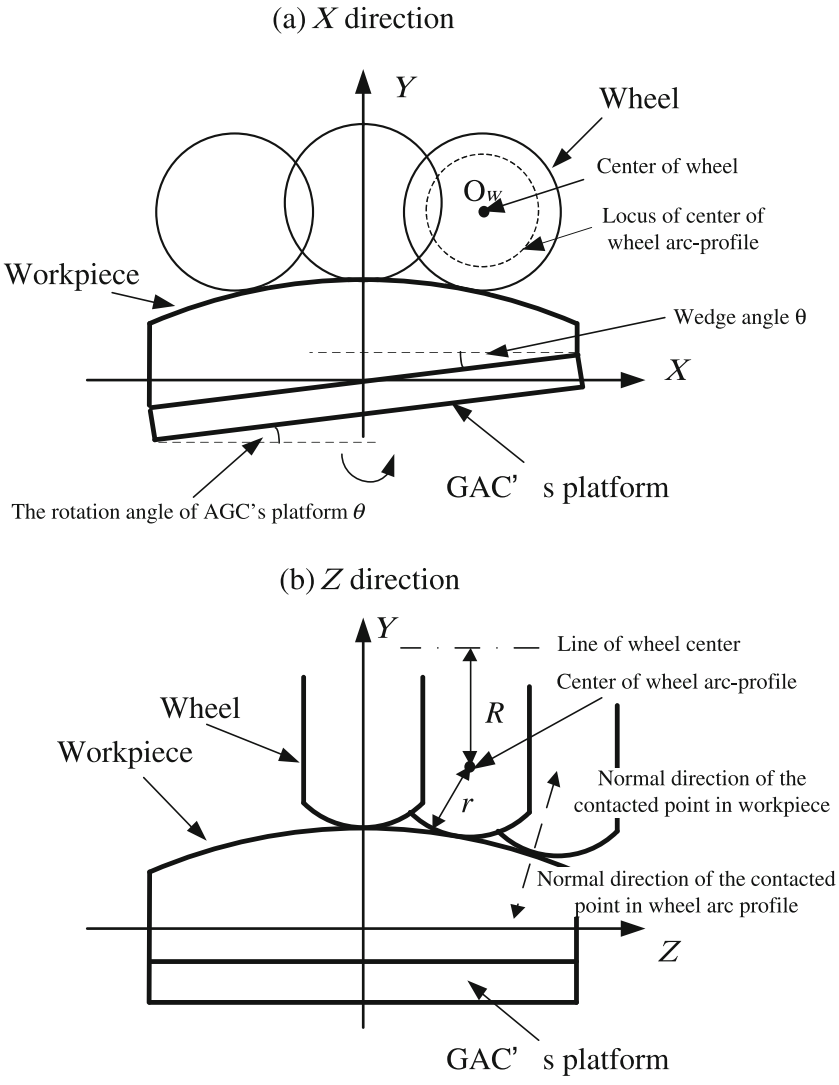

Fig. 3 Parallel grinding using the AGF. **a** *X* direction. **b** *Z* direction

In parallel grinding, the paths of interpolation points on the aspheric surface are planned with the invariable feed length according to the beeline grating method as shown in Fig. 4. Using the paths of interpolation points, the tool paths are then calculated by the geometry of parallel grinding method that will be introduced in the Section 3.3. Owning to the parallel grinding method, the tool paths present an anamorphic camber grating shape as shown in Fig. 4.

3 Error analysis of parallel grinding using the AGF

In the machining process, error in installing a workpiece affects the machining accuracy. Additionally, because of the inverse clearance of the rotational axis, the locking devices of the AGF produce a rotation error for the axes. To ensure machining accuracy, the machining interpolation error and the machining profile error are analyzed according to the error for the AGF.

3.1 Interpolation error calculation

In the linear interpolation, the interpolation errors along the X axis, caused by the installation error of the workpiece and the rotation error of the AGF, are discussed as follows. In the workpiece coordinate system XOY, two adjacent grinding points at the machining locus are shown in Fig. 5. $A(x_i, y_i)$ is the ith interpolation point and $B(x_{i+1}, y_{i+1})$ is the next interpolation point. The line AB is the actual grinding locus from A to B in parallel grinding from linear interpolation. However, the target locus is the arc AB. Therefore, the grinding error along the X axis δ_x is represented by CD, where C is the midpoint of the line AB, and D is the point of intersection of the arc AB and the extended line of O_1C [10]. The grinding error along the X axis δ_x is obtained geometrically and is expressed as:

$$\delta_x = R_x - \sqrt{R_x^2 - \frac{dx^2}{4} - \frac{1}{4}\left(\sqrt{R_x^2 - (x_i + dx)^2} - \sqrt{R_x^2 - x_i^2}\right)^2}, \quad (4)$$

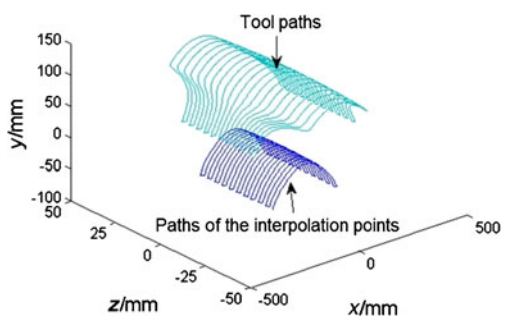

Fig. 4 3D tool paths of parallel grinding

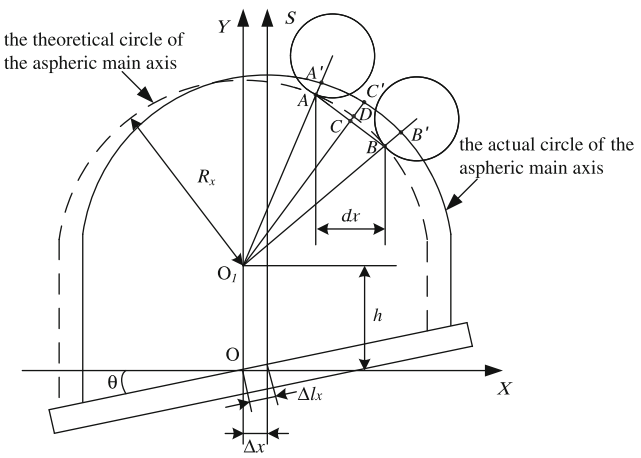

Fig. 5 Error in the installation along the X axis

where dx is the feed length, x_i is the X coordinate of the ith interpolation point, and R_x is the basic radius of the non-axisymmetric aspheric main axis.

In the workpiece coordinate system, the main optical axis S of the NNAL, which should overlap with the Y axis, is orthogonal with the X axis. However, as shown in Fig. 5, the main optical axis S is shifted along the X axis because of the installation error of the workpiece Δl_x. This can be represented as a position error of the main optical axis along the X axis Δx, which affects the machining accuracy. As shown in Fig. 5, the targeted locus of grinding is tilted to arc $\overline{A'B'}$ owing to the installation error of the workpiece Δl_x. The actual grinding error along the X axis δ_x thus changes from CD to $\overline{CC'}$, where C' is the intersection point of the extended line of $\overline{CD}$ and the circle of the aspheric main axis. The new δ_x, which is affected by the position error of the main optical axis along the X axis Δx, can be recalculated according to geometry as follows.

1. In the workpiece coordinate system XOY, the theoretical circle of the aspheric main axis is expressed according to Eq. 1:

$$x^2 + (y + R_x - h)^2 = R_x^2. \quad (5)$$

2. Owing to the installation error Δl_x, the circle of the aspheric main axis is shifted along the X axis. Therefore, the new circle of the aspheric main axis is obtained and is expressed as:

$$(x - \Delta x)^2 + (y + R_x - h)^2 = R_x^2, \quad (6)$$

where Δx is calculated according to

$$\Delta x = \Delta l_x \cdot \cos\theta. \quad (7)$$

3. The point $C(x_c, y_c)$ can be calculated employing the geometrical method and is written as:

$$\begin{cases} x_c = x_i + dx/2 \\ y_c = \left(\sqrt{R_x^2 - x_i^2} + \sqrt{R_x^2 - (x_i + dx)^2}\right)/2 + h \end{cases}, \tag{8}$$

where h is the basic height of the NNAL. The point O_1 is the center of the theoretical circle of the aspheric main axis and is written as $O_1(0, h)$. Therefore, the formula for the line O_1C can be obtained from the coordinates of these two points:

$$y = \frac{\sqrt{R_x^2 - x_i^2} + \sqrt{R_x^2 - (x_i + dx)^2}}{2x_i + dx} x + h. \tag{9}$$

Since $C'(\mathrm{x'_c}, \mathrm{y'_c})$ is the intersection point of the line O_1C and the actual circle of the aspheric main axis, the length of CC', which is the grinding error along the X axis δ_x, can be written as:

$$\delta_x = \sqrt{(x'_c - x_c)^2 + (y'_c - y_c)^2}, \tag{10}$$

where $C'(\mathrm{x'_c}, \mathrm{y'_c})$ is calculated using Eqs. 6 and 8. Therefore, the new value of δ_x can be obtained from Eqs. 6, 8, 9, and 10.

In parallel grinding using the AGF, because of the rotation error of the AGF about the Z axis $\Delta\beta$, the targeted locus of grinding is tilted to arc $\overline{A'B'}$ as shown in Fig. 6. Thus, the actual grinding error of the X axis δ_x changes from CD to $\overline{CC'}$, where C' is the intersection point of the extended line of $\overline{CD}$ and the circle of the aspheric main axis. The new δ_x, which is affected by the rotation error of the AGF, can be recalculated according to the geometry. The calculation method is almost the same as that for the previous δ_x affected by the position error of the main optical axis along the X axis Δx, except that step (2) of the method is modified as follows.

The coordinate system XOY is tilted to the coordinate system $X'OY'$ through an angle $\Delta\beta$. The relationship between these two coordinates is

$$\begin{cases} x' = \mathrm{x} \times \cos(\Delta\theta) - \mathrm{y} \times \sin(\Delta\theta) \\ y' = \mathrm{y} \times \cos(\Delta\theta) + \mathrm{x} \times \sin(\Delta\theta) \end{cases}. \tag{11}$$

Therefore, the revolving actual circle of the aspheric main axis is obtained and is written as

$$(x \times \cos(\Delta\beta) - y \times \sin(\Delta\beta))^2 + (y \times \cos(\Delta\beta) + \cdots \\ x \times \sin(\Delta\beta)R_x - h)^2 = R_x^2. \tag{12}$$

3.2 Shape error

To ensure machining accuracy, the effect of the rotation error of the AGF and the installation error of the workpiece on the machining shape error is analyzed. At the same time, the compensation algorithm for the machining locus of the wheel's center is presented. In machining, the installation errors of a workpiece can be directly compensated for by the tool setting program.

The shape error resulting from the rotation errors of the AGF can be analyzed geometrically. As shown in Fig. 7, M is an interpolation point on a workpiece surface under an ideal condition. However, owing to rotation errors, the actual interpolation point changes from M to M'. Assure that M_i is the aggregate of all theoretical interpolation points and M'_{i} is the aggregate of actual interpolation points. Their relationship is obtained according to homogeneous coordination transformation matrices as follows.

1. Assure that T_z, T_x, and T_y are the rotation matrices for the Z, X, and Y axes, respectively. Thus,

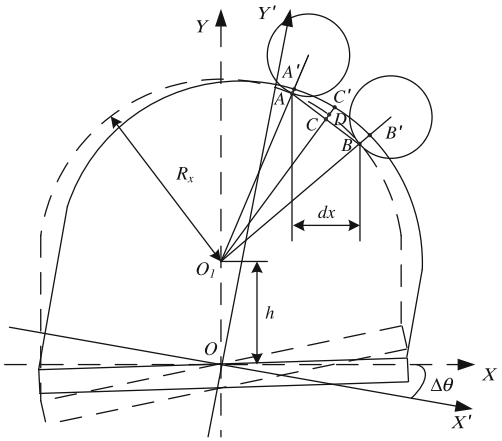

Fig. 6 Rotation error of the A axis

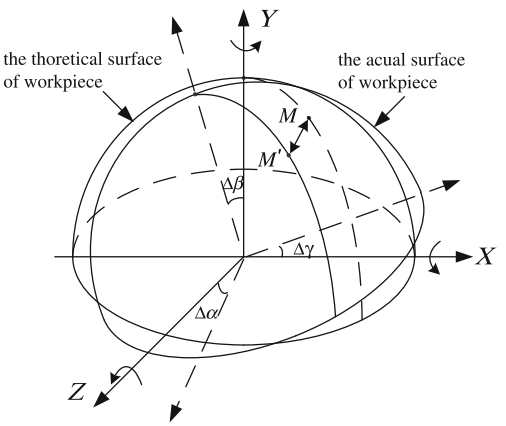

Fig. 7 Shape error

$$T_z = \begin{bmatrix} 1 & 0 & 0 \\ 0 & \cos(\Delta\beta) & -\sin(\Delta\beta) \\ 0 & \sin(\Delta\beta) & \cos(\Delta\beta) \end{bmatrix}, \quad (13)$$

$$T_x = \begin{bmatrix} \cos(\Delta\alpha) & 0 & -\sin(\Delta\alpha) \\ 0 & 1 & 0 \\ \sin(\Delta\alpha) & 0 & \cos(\Delta\alpha) \end{bmatrix}, \quad (14)$$

$$T_y = \begin{bmatrix} \cos(\Delta\gamma) & -\sin(\Delta\gamma) & 0 \\ \sin(\Delta\gamma) & \cos(\Delta\gamma) & 0 \\ 0 & 0 & 1 \end{bmatrix}, \quad (15)$$

where $\Delta\alpha$, $\Delta\gamma$, and $\Delta\beta$ are the rotation errors about the A, B, and C axes.

2. The homogeneous transformation matrix T is expressed as

$$T = T_z \cdot T_x \cdot T_y = \begin{bmatrix} \cos(\Delta\gamma)\cos(\Delta\alpha) & -\cos(\Delta\beta)\sin(\Delta\alpha) & \sin(\Delta\beta) \\ \sin(\Delta\gamma)\sin(\Delta\beta)\cos(\Delta\alpha)+\cos(\Delta\gamma)\sin(\Delta\alpha) & -\sin(\Delta\gamma)\sin(\Delta\beta)\sin(\Delta\alpha)+\cos(\Delta\gamma)\cos(\Delta\alpha) & -\sin(\Delta\gamma)\cos(\Delta\beta) \\ -\cos(\Delta\gamma)\sin(\Delta\beta)\cos(\Delta\alpha)+\sin(\Delta\gamma)\sin(\Delta\alpha) & \cos(\Delta\gamma)\sin(\Delta\beta)\sin(\Delta\alpha)+\sin(\Delta\gamma)\cos(\Delta\alpha) & \cos(\Delta\gamma)\cos(\Delta\beta) \end{bmatrix}. \quad (16)$$

3. The relationship between M and M' is obtained as:

$$M'_{\mathrm{i}} = T \cdot M_i. \quad (17)$$

Therefore, the root mean square (RMS) of the shape error of the workpiece, which results from rotation error, can be simulated using the coordinates of M' and the formula for the nonaxisymmetric aspheric surface of the workpiece.

3.3 Error compensation

To compensate the machining error resulting from the rotation errors, the primary locus of the wheel's center in parallel grinding must be modified. The rotation errors of the AGF can be compensated for by the algorithm as follows:

1. As shown in Fig. 8, the primary wheel center shifts from N to N' in the machining process owing to rotation errors. We let $N'(x_g, y_g, z_g)$ be the compensated wheel center. From Eq. 16, M' can be calculated using M.
2. According to the geometry, the relation between $N'(x_g, y_g, z_g)$ and $M'(x_0, y_0, z_0)$ can be written as:

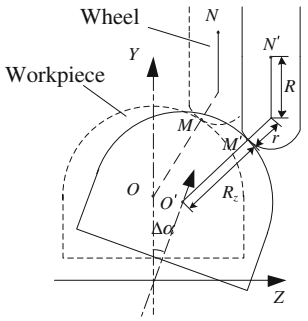

Fig. 8 Compensation for a wheel center

$$\begin{cases} x_g = x_0 - \dfrac{a}{I_r}r - \dfrac{a}{I_R}R \\ y_g = y_0 - \dfrac{b}{I_r}r - \dfrac{b}{I_R}R, \\ z_g = z_0 - \dfrac{c}{I_r} \end{cases} \quad (18)$$

where r is the arc radius of the wheel, R is the basic radius of the wheel, and a, b, c, I_r, and I_R are obtained using

$$\begin{cases} a = -\partial y/\partial x \\ b = 1 \\ c = -\partial y/\partial z \\ I_r = \sqrt{a^2+b^2+c^2} \\ I_R = \sqrt{a^2+b^2}. \end{cases} \quad (19)$$

3. The compensated coordinates of the wheel center $N'(x_g, y_g, z_g)$ are calculated using Eqs. 18 and 19.

4 Simulation and discussion

In this section, simulations and discussions about the grinding errors are presented according to the error analysis in the previous section. The machining conditions in the simulations are presented in Table 1.

4.1 Interpolation error simulation

The effect of the rotation error of the AGF $\Delta\beta$ on the interpolation error along the X axis δ_x is analyzed using a differentiated value of the feed length dx as in Eqs. 8, 9, 10, and 14. The effects of the AGF rotation error $\Delta\beta$ and the feed length dx on the interpolation error along the X axis δ_x are shown in Fig. 9. As $\Delta\beta$ varies from 0° to 0.1° and dx from 0.005 to 3 mm, δ_x varies from almost 0 to 0.048 mm. The simulation shows that the AGF rotation error has a greater effect than the feed length dx on δ_x in the above range.

Table 1 Machining conditions in simulation

Wheel width, B/mm	Basic radius, R/mm	Arc radius, r/mm	Feed depth (mm)	X axis radius, R_x/mm	Z axis radius, R_z/mm	Optical parameter, k	Aspheric parameters, A~F
20	65	35	0.5–2	225	65.95	0.45	6.8×10^{-4}~1.1×10^{-22}

The effect of the fixture rotation error $\Delta\beta$ on the interpolation error along the X axis δ_x varies according to the X coordinate of the workpiece. As shown in Fig. 10, as $\Delta\beta$ varies from 0° to 0.1° and x from 0 to 150 mm, δ_x varies from almost 0 mm to more than 0.1 mm. The simulation shows that the edge of the aspheric lens is the position within the NNAL with maximum δ_x.

4.2 Shape error simulation

The interpolation points M_i are tilted to M'_i owing to the AGF rotation errors $\Delta\alpha$ and $\Delta\beta$, which cause the machined profile of workpiece to deviate from the theoretical aspheric surface. The deviation points M'_i are obtained using Eq. 17. Therefore, the shape error RMS difference of the workpiece between M'_i and the theoretical aspheric surface is simulated as shown in Fig. 11. The simulation shows that the rotation error of the AGF's C axis $\Delta\beta$ has a greater effect than the rotation error of the A axis $\Delta\alpha$ on the shape RMS error because the workpiece is much longer along the X axis than along the Z axis.

5 Experiment

A series of experiments were performed on the grinding machine (MGK7160) developed in previous work to verify the parallel grinding using the AGF and the compensation algorithm. An optical glass (BK7) was selected as the experimental material. To reduce the impact of wheel wear on machining accuracy, a new form-truing process was performed with the same truing conditions to produce a new wheel arc profile. After that, the last wheel arc profile and its arc radius and basic radius were measured to plan new tool paths and to conduct last CNC grinding operation. An inductance micrometer of contact measure was used for measuring the wheel arc profile, and the arc radius and the basic radius of wheel were obtained by round fitting using the measured data. After machining the NNAL, the ground workpiece was unloaded from the grinding machine and the shape accuracy of ground surface was measured using the 3D coordinate measurement machine. In measurement, Y coordinates of the workpiece surface were measured on the point lattice 61×11 mm of Z–X plane. To evaluate the profile accuracy of ground surface, the shape errors were obtained by surface fitting using the measured data. The rough grinding and fine grinding were usually preformed for the experiments and the machining conditions are shown in Table 2.

5.1 Rotation error compensation

In the primitive machining, the radius of the wheel arc profile was 34.3459 mm and the basic radius of the wheel was 165.0544 mm. The shape error of the primitive machining workpiece is shown in Fig. 12. It is noted that the shape error RMS reaches 7.3343 μm and the peak-to-valley (PV) value reaches 35.6753 μm. The locking devices of the AGF produced a 0.0192° rotation error on the C axis, which was measured by a laser interferometer. After the arc wheel was dressed, the second machining for compensating rotation error was carried out using the proposed compensation algorithm. The parameters of compensation machining were same as that of the primitive machining, except the radius of wheel arc profile is 34.3315 mm and the basic radius of wheel is 164.9176 mm by fitting the measured data. As

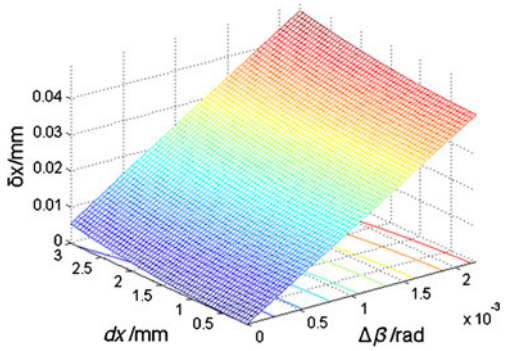

Fig. 9 Effects of $\Delta\beta$ and dx on interpolation error

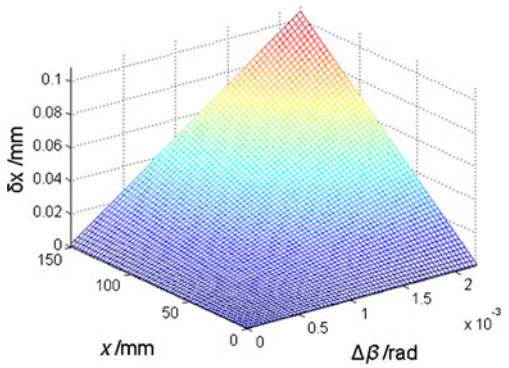

Fig. 10 Effects of $\Delta\beta$ and x on interpolation error

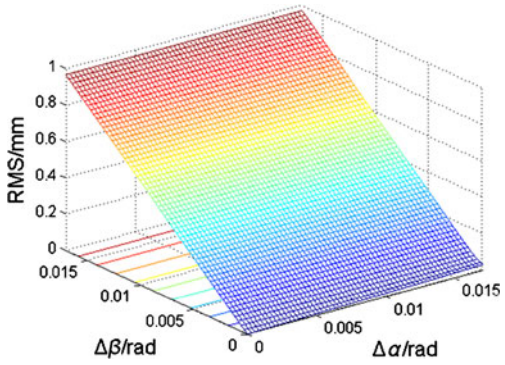

Fig. 11 Effects of $\Delta\alpha$ and $\Delta\beta$ on the profile error of workpiece

shown in Fig. 13, the shape error RMS decreased to 1.1343 μm and the PV decreased to 5.3423 μm after the *C* axis rotation error of the AGF was compensated in the second machining. The experiments show that the machining accuracy is remarkably improved by the compensation algorithm.

5.2 Influences of grinding parameter

Three machining tests were conducted to investigate the machining accuracy with different rotation errors. To reduce the impact of wheel wear on machining accuracy, the arc wheel was dressed before each machining test, too. Figure 14 illustrates the simulated curve of the shape error RMS, which are obtained using a differentiated value of the rotation errors as in Eq. 17. The measured shape errors RMS 2.5422, 4.4988, and 7.3445 μm are obtained when 0.0045°, 0.012°, and 0.018° *C* axis rotation errors are produced, respectively. It is noted that the shape errors RMS are positioned around the simulated curve. It is means that this simulated curve can give a proper description about the trend of the shape error when the rotation errors are not compensated. Furthermore, the rotation error of the AGF is a major factor that influences the machining accuracy compared with other machining parameters.

Other three machining tests using a differentiated value of the feed length *dx* were conducted to compare the effects of grinding parameters and computer mode parameters on the shape errors of aspheric surface. The locking devices of the AGF produced a 0.0241° rotation error on the *C* axis,

Table 2 Machining conditions of experiments

Conditions	Rough grind	Fine grind
Wheel speed (rpm)	1,500	1,500
Feed rate (mm/min)	4,000	4,000
Depth of cut (μm)	30	5
Grinding wheel	Resin Diamond-D91	Resin Diamond-D15
Wheel width (mm)	20	20

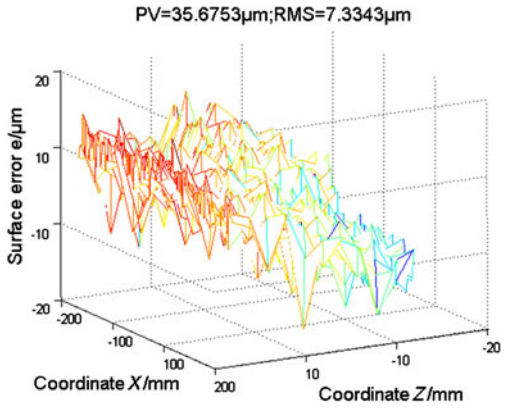

Fig. 12 Primary machining result

which was measured by a laser interferometer. Machining NC code with compensating rotation error was produced by the proposed method. Figure 15 shows the results of three machining tests using the differentiated value of feed length *dx* which are 1, 1.5, and 2 mm, respectively. Note that the measured shape errors RMS are far from the theoretic model

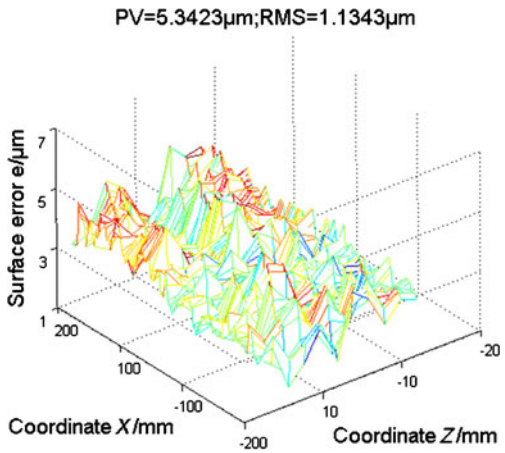

Fig. 13 Compensation machining result

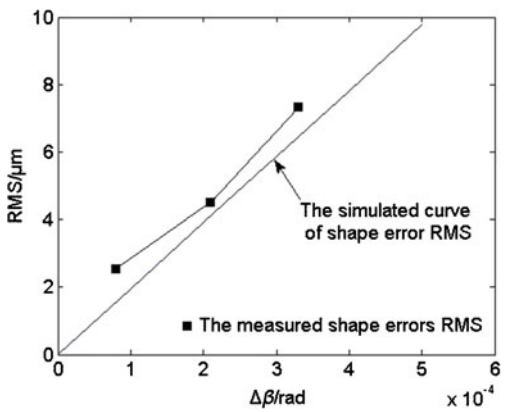

Fig. 14 Machining result without compensating

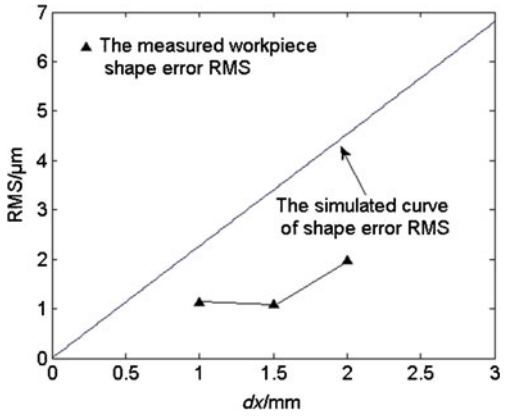

Fig. 15 Compensation machining result using different *dx*

curve. Compared with machining results without compensating rotation errors, the simulation model does not work when the rotation error is compensated. It means that the compensation algorithm corrects the effect of rotation error on the shape error effectively while the rotation error is a major influence factor relative to others machining parameters. The results of experiments show that the compensation algorithm insures the machining accuracy when the AGF is used.

6 Conclusions

In this paper, the AGF was developed for machining an NNAL specifically with a three-axis grinding machine, and the error analysis of the AGF for parallel grinding was presented. The following conclusions can be drawn:

1. The effects of the rotation error of the AGF on the profile accuracy of the workpiece are remarkable in parallel grinding. The simulation results show that the fixture rotation error has a greater effect than the machining parameters, such as the feed length *dx*, on the interpolation error. Owing to the shape of the workpiece, the rotation error of the *C* axis $\Delta\beta$ has a greater effect than the rotation error of the *A* axis $\Delta\alpha$ on the shape error of the workpiece.
2. The experiments show that the shape error of the workpiece is remarkably reduced employing the proposed compensation method, and the proposed grinding method using the AGF is used for machining the NNAL effectively.

Acknowledgments The authors gratefully acknowledge the 863 National High Technology Project (No.2008AA042501) of China by which the paper was supported.

References

1. Park H (2004) A solution for NURBS modelling in aspheric lens manufacture. Int J Adv Manuf Technol 23(1–2):1–10. doi:10.1007/s00170-002-1518-5
2. Sung IK, Oh CJ, Lee ES, Kim OH (2006) A swing arm method for profile measurement of large optical concave surfaces in the lapping process. Int J Adv Manuf Technol 29:113–117. doi:10.1007/s00170-004-2473-0
3. Sun W, McBride JW, Hill M (2010) A new approach to characterising aspheric surfaces. Precis Eng 34:171–179
4. Shibuya A, Arai Y, Yoshikawa Y, Gao W, Nagaike Y, Nakamura Y (2010) A spiral scanning probe system for micro-aspheric surface profile measurement. Int J Adv Manuf Technol 46:845–862
5. Rhee HG, Kim DI, Song JB, Lee HJ, Lee YW, Jo JH (2011) Performance evaluation of laser lithographic machine for computer-generated hologram. Int J Adv Manuf Technol 52(9–12):1005–1009. doi:10.1007/s00170-010-2803-3
6. Chen MJ, Li D, Dong S (2002) Research on a large depth-to-diameter ratio ultra-precision aspheric griding system. J Mater Process Tech 129:91–95
7. Cheng HB, Feng ZJ, Cheng K, Wang YW (2005) Design of a six-axis high precision machine tool and its application in machining aspherical optical mirrors. Int J Mach Tools Manuf 45:1085–1094
8. Lee ES, Baek SY (2007) A study on optimum grinding factors for aspheric convex surface micro-lens using design of experiments. Int J Mach Tools Manuf 47:509–520
9. Xie J, Xu WW, Tamaki J (2007) 3D simulation of arc envelope grinding of non-axisymmetric aspheric surface. Int J Mach Machin Mater 2:85–96. doi:10.1504/IJMMM.2007.012669
10. Xie J, Zhou RM, Xu J, Zhong YG (2010) Form-truing error compensation of diamond grinding wheel in CNC envelope grinding of free-form surface. Int J Adv Manuf Technol 48:905–912. doi:10.1007/s00170-009-2338-7
11. Lee TM, Lee EK, Yang MY (2007) Precise bi-arc curve fitting algorithm for machining an aspheric surface. Int J Adv Manuf Technol 31:1191–1197. doi:10.1007/s00170-005-0290-8
12. Chen FJ, Yin SH, Huang H, Ohmori H, Wang Y, Fan YF, Zhu YJ (2010) Profile error compensation in ultra-precision grinding of aspheric surfaces with on-machine measurement. Int J Mach Tools Manuf 50:480–486
13. Saeki M, Lee J, Kuriyagawa T, Syoji K (2001) Machining of aspherical opto-device utilizing parallel grinding method. The 16th ASPE Annual Meeting, USA, 25: 433–436
14. Hwang Y, Kuriyagawa T, Lee SK (2006) Wheel curve generation error of aspheric microgrinding in parallel grinding method. Int J Mach Tools Manuf 46:1929–1933